Canonicalization of projected entangled pair states

R. Haghshenas,[1] Matthew J. O'Rourke,[1] and Garnet Kin-Lic Chan[1]

[1] *Division of Chemistry and Chemical Engineering, California Institute of Technology, Pasadena, California 91125, USA*

We propose a simple algorithm to convert a projected entangled pair state (PEPS) into a canonical form, analogous to the well-known canonical form of a matrix product state. Our approach is based on a variational gauging ansatz for the QR tensor decomposition of PEPS columns into a matrix product operator and a finite depth circuit of unitaries and isometries. We describe a practical initialization scheme that leads to rapid convergence in the QR optimization. We explore the performance and stability of the variational gauging algorithm in norm calculations for the transverse-field Ising and Heisenberg models on a square lattice. We also demonstrate energy optimization within the PEPS canonical form for the transverse-field Ising model. We expect this canonical form to open up improved analytical and numerical approaches for PEPS.

PACS numbers: 75.40.Mg, 75.10.Jm, 75.10.Kt, 02.70.-c

Introduction—Tensor network states (TNS)[1–5] are widely used as variational wave functions to approximate low-energy states of quantum many-body systems[6,7]. Their power arises from their ability to efficiently capture global behaviors of quantum correlations in the system, as described by entanglement area laws[8,9]. As a consequence, the global wave function is encoded in local tensors with finite bond dimension. A concrete example is the matrix product state (MPS)[10–13], a class of tensor-network states that capture the area law in 1D, and which underlie the success of the density matrix renormalization group (DMRG)[1,2].

The local tensors in a TNS are not uniquely defined and contain redundant parameters known as a local gauge. In MPS, such gauges can be fixed by bringing the MPS into a canonical form where all tensors but one are isometric[13]. The canonical form is simple to compute through QR decompositions, and has many applications, such as in defining optimal local truncations[13,14], the DMRG algorithm, constructing the tangent space of excitations[15–18], and providing a framework to characterize phases[19,20].

Projected entangled pair states (PEPS)[7,21–23] are higher-dimensional generalizations of MPS with analogous area laws. The PEPS has widely been used as a variational ansatz to explore physical properties of quantum many-body systems[24–30]. It has already been observed that partially fixing the gauge of local tensors can dramatically improve the efficiency and stability of PEPS algorithms[31–34]. However, unlike in MPS, computing a fully canonical form for a PEPS remains a challenge.

Here, we introduce a gauging variational ansatz that efficiently brings a PEPS wave function into a full canonical form in direct analogy with that of an MPS. To do so, we re-express the columns of the PEPS as a QR tensor product, where Q is an isometric column tensor and R is a matrix product operator (MPO). We show that Q can be compactly parametrized by a finite-depth circuit of block isometries and unitaries that can be determined by variational optimization. After transforming all columns but one (a central column) to be isometric, we obtain the (column) canonical form of the PEPS, where part of the entanglement in the environment is transferred to the central column. We explore the stability and performance of the QR decomposition and PEPS canonical representation in calculating the norm in the 2D transverse-field Ising (ITF) and Heisenberg models on a square lattice. We analyze the behavior of imaginary-time energy optimization in the canonical PEPS form in the context of the ground-state of the transverse-field Ising model.

PEPS definition and background.—A PEPS is a TNS defined by a set of local tensors $\{A_i^{s_i}\}$ connected by virtual bonds along the bonds of the physical lattice. The bond dimension of the virtual bonds is denoted D, which controls the number of parameters (or, more physically, the amount of entanglement in the wavefunction) and hence the accuracy of the ansatz. The physical indices s_i encode the local physical Hilbert space of dimension d. A PEPS wave function $|\Psi\rangle$ on the $l_x \times l_y = 4 \times 4$ square lattice with open boundary conditions is depicted in Fig. 1(a),

$$|\Psi\rangle = \sum_{\{s_i\}} \mathcal{F}(A_1^{s_1}, A_2^{s_2}, \cdots, A_{l\times l}^{s_{l\times l}})|s_1, s_2 \cdots, s_{l\times l}\rangle \quad (1)$$

where $\mathcal{F}$ denotes tensor contraction of the virtual bonds.

The tensor contraction in Eq. (1) is invariant under insertion of a gauge matrix and its inverse G, G^{-1} between two tensors (along with a virtual bond). In an MPS, the canonical form at site i is defined as the choice of gauges such that the environment tensor $\mathcal{G}_i$ (constructed by partial norm-contraction over all sites except i) is the identity tensor

$$\mathcal{G}_i = \mathcal{F}\left(\prod_{j\neq i} E_j\right) = \mathbb{1} \quad (2)$$

with $E_j = \sum_{s_j} A_j^{s_j\dagger} A_j^{s_j}$. By ensuring that the PEPS tensors satisfy Eq. (2), it also defines an analogous canonical form for a PEPS, depicted in Fig. 1(b). In the case of an

MPS, we can convert an arbitrary MPS into canonical form by sequential QR (LQ) decompositions of tensors to the left (right) of site i, $A_j^{s_j} \to Q_j^{s_j} R_j$ ($A_j^{s_j} \to L_j Q_j^{s_j}$) where Q_j is orthogonal in the sense $\sum_{s_j} Q_j^{s_j\dagger} Q_j^{s_j} = \mathbb{1}$ (for LQ, $\sum_{s_j} Q_j^{s_j} Q_j^{s_j\dagger} = \mathbb{1}$). For simplicity, we henceforth do not distinguish between QR and LQ, with the choice implicit from the diagrammatic representation. R_j is then absorbed into the adjacent tensor for the subsequent QR decomposition until the full canonical form is reached.

PEPS canonical form and column QR ansatz—To similarly canonicalize a PEPS, we sequentially decompose the PEPS columns, denoted M (composed of tensors $\{m_i\}$), as a QR tensor contraction, where the column tensor Q is isometric, satisfying $Q^\dagger Q = \mathbb{1}$, see Fig. 1(c, d). The gauge column tensor R (composed of tensors $\{r_i\}$) is an MPO acting on the horizontal virtual bonds. Once all columns (around a central column) are decomposed to be isometric, the central column C can be viewed as an MPS by grouping the horizontal bonds with the physical bonds. This central column can then be canonicalized around a chosen site using the MPS canonicalization algorithm above, to yield a complete PEPS canonicalization (Fig. 1(e)). Note that the PEPS canonicalization condition around a site (Fig. 1(b)) does not itself specify that columns to the left and right of the central column separately contract to the identity; the conditions we impose are thus sufficient and convenient when canonicalizing a PEPS, but are more constrained than the necessary conditions for Fig. 1(b).

To explicitly carry out the QR decomposition, we first rewrite M and thus Q as MPOs by fusing physical bonds with the left virtual bonds (Fig. 1(f)). Then, to explicitly enforce the isometric constraint on Q, we write it as a finite depth-n circuit of block-size l isometries and unitaries $\{u_i\}$, where the isometries appear in the edge layer of the circuit (Fig. 1(g))[35,36]. The layer depth and block size control the distribution of entanglement between Q and R. In practice, to obtain a faithful QR decomposition we have found it sufficient to use $n = 2$, increasing l if necessary.

To determine the tensors in the QR ansatz, we minimize the distance (cost function) $F = \| M - Q(\{u_i\})R(\{r_i\}) \|$ with respect to $\{u_i, r_i\}$ ($\| \cdot \|$ is the Hilbert-Schmidt norm) using standard tensor network techniques[37–39]. We optimize the tensors one at a time and sweep until convergence. The cost function depends quadratically on $\{r_i\}$, i.e. $F = r_i^\dagger N r_i - S r_i + \text{const}$, which is explicitly minimized by solving the linear equation $N r_i' = S$ (which can be solved iteratively with a method such as conjugate gradient, with a cost of $\mathcal{O}(D^8)$ per iteration). To update the isometric/unitary tensors $\{u_i\}$, we observe that the cost function only depends linearly on them due to cancellations, i.e. $F = u_i^\dagger Y + \text{const}$, thus the optimal solution is given by $u_i' = -VU^\dagger$, where V, U appear in the singular value decomposition $Y = UsV^\dagger$[37]. The tensor network diagrams of tensors N, S and Y appear in Fig. 1(h).

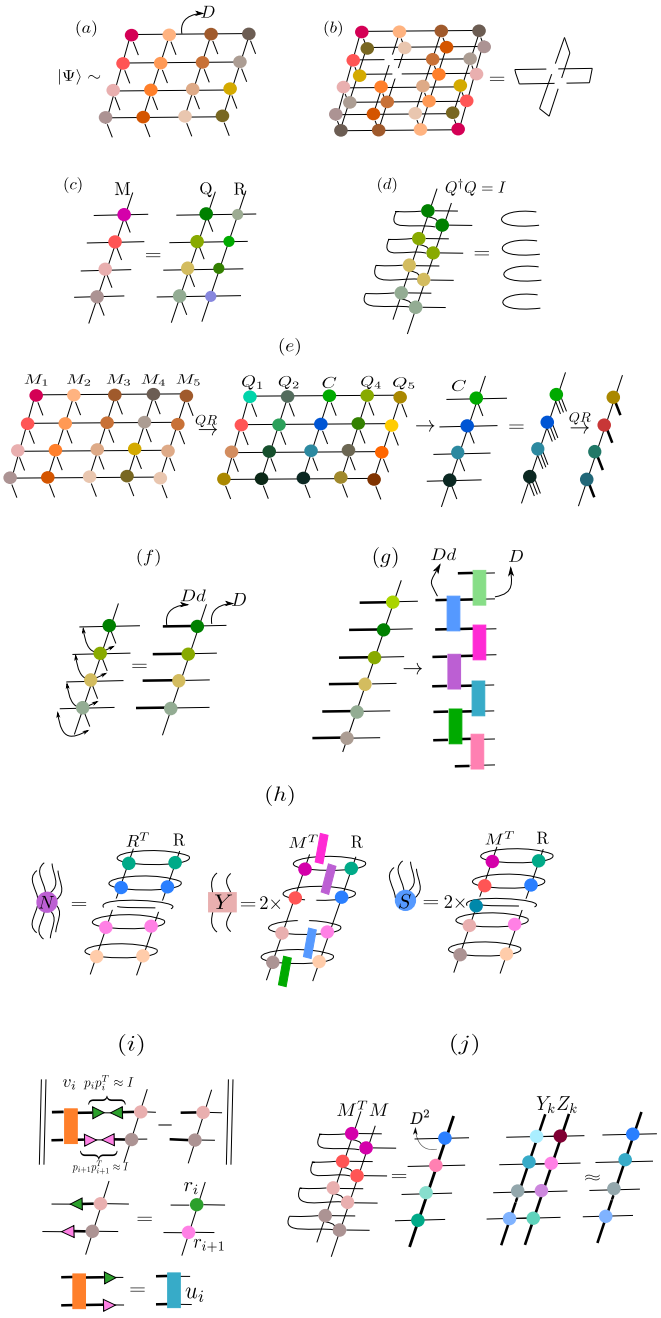

FIG. 1. (Color online) (a) Tensor-network representation of the PEPS $|\Psi\rangle$ on a 4×4 square lattice with open boundary conditions. (b) A PEPS canonicalized up to a single site, hence the environment around that site contracts to identities. (c) A decomposition of a bulk column $M \approx QR$, where (d) tensor Q is isometric, i.e. $Q^\dagger Q = \mathbb{1}$. (e) The graphical representation of steps based on our QR scheme to bring a PEPS into canonical form. Note in a final step (not shown), MPS canonicalization is used on the central column C. (f) The tensor Q is reshaped into an MPO by fusing the virtual bond and physical bond as shown by arrows. The thick virtual bonds have bond dimension Dd. (g) The isometric tensor Q is parameterized by a finite depth circuit of l-site isometries/unitaries $\{u_i\}$. (h) Tensor-network representation of environment tensors N, S and Y appearing in the QR optimization procedure. (i) The local distance (cost function) used to obtain a good initial guess for local tensors u_i, r_i and r_{i+1}. The cost function is minimized with respect to tensors p_i, p_{i+1} and v_i, which are used to build u_i, r_i and r_{i+1} as depicted. (j) The graphical representation of $M^\dagger M$ and $Y_k Z_k$ used in the Schulz algorithm.

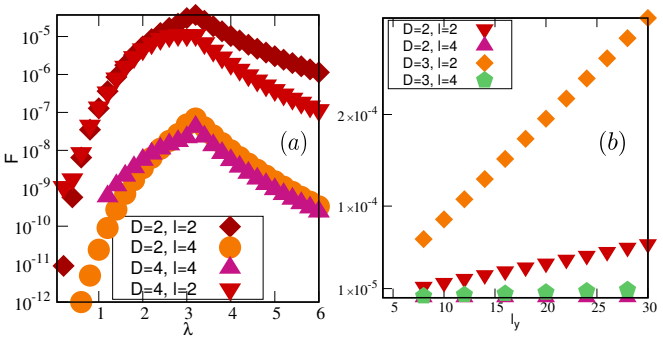

FIG. 2. (Color online) Accuracy of the variational ansatz for QR decomposition of a single bulk column. (a) The relative distance F as a function of transverse Ising field λ, for a single bulk column with $l_y = 16$, and for given values of bond dimension D and block size l used in Q. The distance F rapidly decreases with increasing l, as more entanglement is included in the Q circuit. (b) The relative distance as a function of PEPS column length l_y for different block sizes l. The error of the variational ansatz increases linearly with the length l_y.

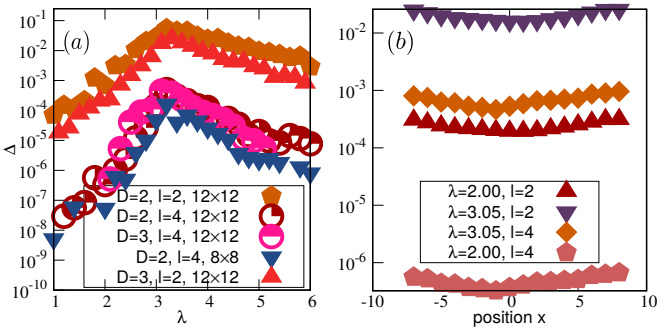

FIG. 3. (Color online) (a) The relative error of the norm contraction $\Delta = \frac{N-N_b}{N_b}$ as a function of transvaerse Ising field λ. N_b is a reference norm obtained by boundary method contraction. For the norm computed via the canonical form, we use $D_c = 4D$. (b) Δ as a function of column position x in the PEPS for different values of λ. The bond dimensions are $D = 3$, $D_c = 12$, and the lattice size is 16×16.

To accelerate the QR optimization (and to avoid local minima) we start with a good initial guess for $\{u_i, r_i\}$. We have used two techniques. The first uses a local projective truncation on the tensors $\{m_i\}$ to initialize $\{u_i\}$ and $\{r_i\}$. To this end, we contract an approximate resolution of the identity (i.e. $\mathbb{1}_D \approx p_i p_i^\dagger$ where p_i is a local isometry) and a unitary v_i into two adjacent tensors m_i, m_{i+1} and optimize p_i, p_{i+1} and v_i to minimize the local cost function shown in Fig. 1(i). Once we have the optimized tensors p_i, p_{i+1} and v_i, we construct a guess for r_i, r_{i+1} and u_i as shown in Fig. 1(i). This initialization is purely local but in practice, we find that it performs well.

A second strategy is based on an accurate estimate of the $\{r_i\}$ tensors using a Schulz iteration for the matrix square-root[40]. Note that R is formally the square root of $M^\dagger M$, due to the isometric property of Q. We thus rewrite $M^\dagger M$ as an MPO as in Fig. 1(j). Then, starting from $Y_0 = M^\dagger M$ and $Z_0 = \mathbb{1}$, the coupled Schulz iteration, $Y_{k+1} = \frac{1}{2} Y_k (3\mathbb{1} - Z_k Y_k)$, $Z_{k+1} = \frac{1}{2}(3\mathbb{1} - Z_k Y_k) Z_k$, gives $Y_{k\to\infty} = R$ and $Z_{k\to\infty} = R^{-1}$. The vertical bond dimension of Y_k and Z_k increases with each MPO multiplication (Fig. 1(j)) thus we perform MPO compression after each iteration (viewing the MPO as an MPS). The final Y_k (R) is compressed back to vertical bond dimension D. Also, since Z_k approximates R^{-1} which may have arbitrarily large norm, we regularize the iteration using $M^\dagger M \to M^\dagger M + \delta I$, where δ is a small number ($\sim 10^{-6}$). The Schulz iteration converges rapidly (see SM) and we use this accurately estimated R to initialize the optimization of the tensors in Q with respect to the cost function F. Although computing the Schulz iteration is more expensive than the local initialization, we expect it to be better when canonicalizing PEPS with more entanglement.

PEPS canonicalization sweep, cost, and truncations— To canonicalize all columns $M^{[1]} M^{[2]} \dots M^{[l_x]}$ in the PEPS, we sweep over all the columns in a prescribed order (say from left to right) and compute the QR decomposition to each. For a single PEPS column of bond dimension D and an $n = 2$, $l = 2$ QR ansatz, the cost of the QR optimization is $\mathcal{O}(l_y D^8)$ (using the iterative cost of solving for $\{r_i\}$). After the column has been converted to QR form, we then absorb the R gauge into the neighboring M column, creating a combined column with an increased vertical bond dimension of D^2. To leading order, the cost of decomposing this by QR optimization is also $\mathcal{O}(l_y D^8)$. Thus the cost of the full canonicalization sweep over columns is $\mathcal{O}(l_x l_y D^8)$.

The above sweep leaves the PEPS in the form $Q^{[1]} Q^{[2]} \dots R^{[l_{x-1}]} M^{[l_x]}$. We can absorb the final gauge into the last PEPS column to make a (rightmost) central column, giving the left canonical form of the PEPS, $Q^{[1]} Q^{[2]} \dots C^{[l_x]}$. Note that canonicalization redistributes entanglement in the PEPS. The above central column C has a formal bond dimension D^2, which we truncate to $D_c > D$ (with cost $\mathcal{O}(l_y D^8)$) to reflect the fact that C must now carry some entanglement that was originally stored in the environment around it. We can perform this column truncation as an MPS truncation with enlarged physical bond dimension $D^2 d$, as the surrounding columns have been canonicalized. Note that an analogous role to D_c is played by χ in PEPS contraction algorithms[33,41,42], but here D_c is an (auxiliary) bond dimension for a single PEPS layer, rather than for a double layer, thus we expect $D_c < \chi$, or potentially even $D_c \propto D$ leading to a reduction of computational cost as found in single-layer PEPS algorithms[43,44]. Finally, the process of compressing the final column C from bond dimension $D^2 \to D_c$ immediately leaves the central column canonicalized up to a single site, as in Fig. 1(b). Shifting this central site along the column can then be done with

subleading cost to the preceding compression steps.

We now discuss the cost to convert between different column canonical forms, which is important to algorithms such as energy optimization. For example, consider moving the central column from l_x to l_{x-1}. First, we perform a QR approximation, $C^{[l_x]} \to R^{[l_x]}Q^{[l_x]}$. Then, we absorb $Q^{[l_{x-1}]}$ into the gauge $R^{[l_x]}$ to form the central column, $Q^{[l_{x-1}]}R^{[l_x]} \to C^{[l_{x-1}]}$, which we truncate to vertical bond dimension D_c. For $n = 2$, $l = 2$, Q is an MPO with vertical bond dimension D^2, thus this appears to be an expensive bond truncation from $D^3 \to D_c$. (Using sequential SVD on the MPS bonds, the cost is $\mathcal{O}(l_y D^{11}) + \mathcal{O}(l_y D^8 D_c)$. If we instead consider direct minimization $|| \, |\phi\rangle - |\psi\rangle ||$ (the cost typically reported in boundary PEPS algorithms) where $|\phi\rangle$ and $|\psi\rangle$ are MPSs with physical bond dimension dD^2 and virtual bond dimensions D^3 and D_C respectively, then the cost is $\mathcal{O}(l_y D^8 D_c) + \mathcal{O}(l_y D^5 D_c^2)$).

The formally large bond dimension of Q is primarily an artifact of expressing the isometric constraint in terms of gates. However, we can use the QR ansatz structure to reduce the cost of this step, by absorbing and truncating first the column of isometries, then the column of unitaries. (In both these truncations, the surrounding columns are canonical, and thus each can be performed as an MPS truncation). With this technique, the cost to move the central column is $\mathcal{O}(l_y D^4 D_c^4) + \mathcal{O}(l_y D^6 D_c^2)$ and $\mathcal{O}(l_y D^4 D_c^4) + \mathcal{O}(l_y D^4 D_c^3)$ (respectively for truncating the column of isometries and unitaries by using direct minimization). For explicit SVD truncation, the leading term is still $\mathcal{O}(l_y D^{11})$, although its prefactor and subleading terms are smaller.

From the above, we see that in computing the canonical form, and in moving the central column, there are two potential sources of error that must be controlled. The first is the error of the QR *approximation error*, controlled by the finite-depth/block-size (n, l) of $\{u_i\}$ and the vertical MPO bond dimension D of R. The second is the *absorption error*, that arises from the truncated vertical bond dimension D_c of the central column. Note that because the canonicalized PEPS has some bonds with different dimension to that in the original PEPS, care must be taken when comparing the cost of canonical and non-canonical PEPS algorithms.

Accuracy of QR ansatz—To assess the accuracy of the QR ansatz, we first study its performance for a single PEPS column. As our initial state, we use the (approximate) ground-state of the spin-$\frac{1}{2}$ ITF model on the square lattice (additional results for the Heisenberg model are in the SM). The ITF model is defined by

$$H_{\mathrm{ITF}} = -\sum_{\langle ij \rangle} \sigma_z^i \sigma_z^j - \lambda \sum_i \sigma_x,$$

where σ_α are the Pauli matrices. This model has a critical point at $\lambda_c \approx 3.05$. Our initial PEPS is constructed from the bulk tensors of an infinite PEPS ground-state[45] (optimized with a full-update scheme[31,42] and a 2×2 unit cell) that is repeated periodically across the finite PEPS lattice.

We measure the accuracy of the QR ansatz by the value of its optimization cost function F. Here, the parameter controlling the accuracy is the block size l of the isometric/unitary circuit (the number of layers is kept as $n = 2$, and the vertical bond dimension of R is kept as D). In Fig. 2(a), we show the plot of the distance F versus ITF magnetic field λ. As expected, when the system is close to criticality, the accuracy is reduced as the ground state becomes more entangled. Increasing l increases the disentangling effect of the unitaries, and the accuracy increases rapidly (we conjecture exponentially with l), especially far from criticality.

Next, we investigate the QR accuracy as a function of system size l_y. As shown in Fig. 2(b), the relative error in F increases linearly with system size, although the slope shows a rapid decay with the isometry/unitary block size l. Thus, the variational gauging ansatz introduces a constant error per lattice site, consistent with a fidelity that goes like $e^{-\epsilon l_y} \sim 1 - \epsilon l_y$.

Accuracy of PEPS canonical form— We next investigate the accuracy and stability of the full PEPS canonical form constructed from a sweep of the QR approximation and absorption steps across the columns. We estimate the faithfulness of the canonical form from the norm contraction $\mathcal{N} = \langle\Psi|\Psi\rangle$, and we use $D_c = 4D$ in the absorption step. We compute the norm in the canonical form using only the central column C since all other columns contract exactly to the identity. The relative error of norm contraction is then defined as $\Delta = \frac{\mathcal{N}-\mathcal{N}_b}{\mathcal{N}_b}$, where the reference value $\mathcal{N}_b$ is obtained using an accurate boundary contraction of the original (uncanonicalized) PEPS keeping a large boundary auxiliary bond dimension[6,22,46]. In Figs. 3(a, b), we show a plot of the relative error Δ as a function of ITF magnetic field λ (using the same approximate ground-state as above) and central column position. Similarly to the single column results above, the accuracy of the full canonical form depends on the correlation length of the model, and the canonicalization error decreases rapidly (exponentially) as the block size l is increased.

Energy optimization in canonical form—A natural application of the PEPS canonical form is to ground-state energy optimization, which mimics the use of the MPS canonical form in energy optimization. To show this, we perform imaginary time evolution on the ITF model, which we carry out with a sequence of gates $e^{-\tau h}$ on the horizontal and vertical bonds[6,33]. Evolution on a column of vertical bonds is conveniently carried out on the central column C of a canonical PEPS with bond dimension D_c, where it reduces to an MPS imaginary time evolution followed by an MPS truncation with an enlarged physical bond dimension D^2d. Evolution on a column of horizontal bonds can be carried out using a two-column canonical PEPS (analogous to the two-site MPS canonical form) where there are two central columns, and columns to the left and right of these two

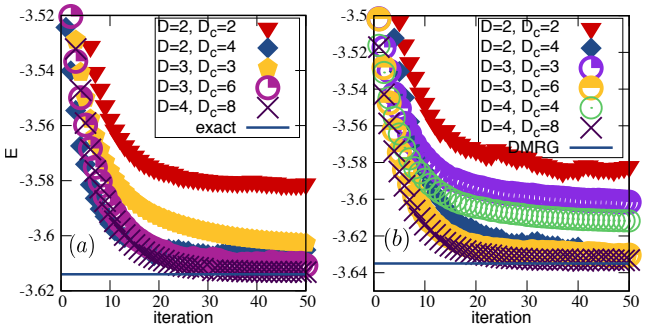

FIG. 4. (Color online) Imaginary time energy optimization based on the PEPS canonical form. The canonical PEPS energy of the ITF model as a function of imaginary time sweep for (a) 4×4 and (b) 8×8 lattices with field $\lambda = 3.5$. The horizonatal DMRG line is the result of a converged 2D DMRG calculation and can be taken to be numerically exact.

are isometric tensors Q, thus reducing the optimization problem to one of a PEPS with only two columns. In this case, rather than canonicalizing the remaining environment around the bond in the two column PEPS, we contract it exactly, which is straightforward. Since there are only two columns, these can be reduced to an MPS with enlarged vertical bond dimension $D^2 D_c$ and physical bond dimension $D^2 d^2$. In Fig. 4(a, b) we show the energy as a function of the number of full imaginary time sweeps for the ITF model at field strength $\lambda = 3.5$ compared to a near-exact DMRG result. Note that both D (which controls the dimension of Q and R) and D_c (vertical bond dimension of the central column) affect the final converged energy; in this setting, increasing D_c has a larger effect than increasing D. The relative error of the energy per site reached for the largest bond dimension $D = 4, D_c = 8$ for both lattice sizes is on the order of 10^{-4}.

Conclusions—In conclusion, we have described a procedure to convert a PEPS into a canonical form analogous to that of an MPS where all columns but one are isometric, by sequentially decomposing columns through a variational QR ansatz. We find that the canonicalization is stable and can be carried out with a small and controllable error. Canonicalization redistributes entanglement in the PEPS, resulting in a central column with increased bond dimension. Our procedure introduces the possibility to formulate canonical PEPS algorithms which make explicit use of an isometric environment, which we demonstrated in an imaginary time optimization of the ground-state energy. However, the redistribution of bond dimensions in the canonical form makes the comparison between canonical and standard PEPS algorithms quite subtle. The QR ansatz we use also suggests an alternative strategy of directly optimizing the underlying network of isometries and unitaries, without explicitly converting into the standard PEPS column-row form. Future investigations will focus on more detailed analysis of these and other algorithms as well as the general representational power of canonicalized PEPS.

Note: As this manuscript was prepared for submission, we were notified of Ref. 47. In that work, the authors similarly pursue a full canonicalization of a PEPS, but use a different set of isometric conditions on the Q tensors which are more constrained than the ones that we use. Further work is needed to understand the relationship between these techniques.

ACKNOWLEDGMENTS

Primary support for this work was from MURI FA9550-18-1-0095. Some of code used to test energy optimization was based on work supported by the US National Science Foundation (NSF) via grant CHE-1665333. MJO acknowledges a US NSF Graduate Research Fellowship via grant DEG-1745301. GKC acknowledges support from the Simons Foundation.

[1] S. R. White, Phys. Rev. Lett. **69**, 2863 (1992).
[2] S. R. White, Physical Review B **48**, 10345 (1993).
[3] G. Vidal, Physical review letters **99**, 220405 (2007).
[4] H. J. Changlani, J. M. Kinder, C. J. Umrigar, and G. K.-L. Chan, Physical Review B **80**, 245116 (2009).
[5] F. Mezzacapo, N. Schuch, M. Boninsegni, and J. I. Cirac, New Journal of Physics **11**, 083026 (2009).
[6] F. Verstraete, V. Murg, and J. Cirac, Advances in Physics **57**, 143 (2008), http://dx.doi.org/10.1080/14789940801912366.
[7] R. Orus, Annals of Physics **349**, 117 (2014).
[8] P. Calabrese and J. Cardy, Journal of Statistical Mechanics: Theory and Experiment **2004**, P06002 (2004).
[9] G. Vidal, J. I. Latorre, E. Rico, and A. Kitaev, Phys. Rev. Lett. **90**, 227902 (2003).
[10] S. Östlund and S. Rommer, Physical review letters **75**, 3537 (1995).
[11] M. Fannes, B. Nachtergaele, and R. F. Werner, Communications in mathematical physics **144**, 443 (1992).
[12] M. Fannes, B. Nachtergaele, and R. Werner, Journal of functional analysis **120**, 511 (1994).
[13] U. Schollwöck, Annals of Physics **326**, 96 (2011), january 2011 Special Issue.
[14] U. Schollwöck, Rev. Mod. Phys. **77**, 259 (2005).
[15] J. J. Dorando, J. Hachmann, and G. K.-L. Chan, The Journal of chemical physics **130**, 184111 (2009).
[16] J. Haegeman, J. I. Cirac, T. J. Osborne, I. Pižorn, H. Verschelde, and F. Verstraete, Physical review letters **107**, 070601 (2011).
[17] N. Nakatani, S. Wouters, D. Van Neck, and G. K.-L. Chan, The Journal of chemical physics **140**, 024108 (2014).

[18] L. Vanderstraeten, M. Mariën, F. Verstraete, and J. Haegeman, Phys. Rev. B **92**, 201111 (2015).
[19] F. Pollmann and A. M. Turner, Phys. Rev. B **86**, 125441 (2012).
[20] C.-Y. Huang, X. Chen, and F. Pollmann, Phys. Rev. B **90**, 045142 (2014).
[21] T. Nishino and K. Okunishi, Journal of the Physical Society of Japan **65**, 891 (1996).
[22] F. Verstraete and J. I. Cirac, arXiv preprint cond-mat/0407066 (2004).
[23] F. Verstraete, M. M. Wolf, D. Perez-Garcia, and J. I. Cirac, Physical review letters **96**, 220601 (2006).
[24] V. Murg, F. Verstraete, and J. I. Cirac, Phys. Rev. B **79**, 195119 (2009).
[25] L. Wang, Z.-C. Gu, F. Verstraete, and X.-G. Wen, Phys. Rev. B **94**, 075143 (2016).
[26] W.-Y. Liu, S. Dong, C. Wang, Y. Han, H. An, G.-C. Guo, and L. He, Phys. Rev. B **98**, 241109 (2018).
[27] B.-X. Zheng, C.-M. Chung, P. Corboz, G. Ehlers, M.-P. Qin, R. M. Noack, H. Shi, S. R. White, S. Zhang, and G. K.-L. Chan, Science **358**, 1155 (2017).
[28] R. Haghshenas, W.-W. Lan, S.-S. Gong, and D. N. Sheng, Phys. Rev. B **97**, 184436 (2018).
[29] R. Haghshenas and D. N. Sheng, Phys. Rev. B **97**, 174408 (2018).
[30] M. J. O'Rourke, Z. Li, and G. K.-L. Chan, Phys. Rev. B **98**, 205127 (2018).
[31] H. N. Phien, I. P. McCulloch, and G. Vidal, Phys. Rev. B **91**, 115137 (2015).
[32] H. N. Phien, J. A. Bengua, H. D. Tuan, P. Corboz, and R. Orús, Phys. Rev. B **92**, 035142 (2015).
[33] M. Lubasch, J. I. Cirac, and M.-C. Bañuls, Phys. Rev. B **90**, 064425 (2014).
[34] G. Evenbly, Phys. Rev. B **98**, 085155 (2018).
[35] F. Pollmann, V. Khemani, J. I. Cirac, and S. L. Sondhi, Phys. Rev. B **94**, 041116 (2016).
[36] T. B. Wahl, A. Pal, and S. H. Simon, Phys. Rev. X **7**, 021018 (2017).
[37] G. Evenbly and G. Vidal, Phys. Rev. B **79**, 144108 (2009).
[38] G. Evenbly, Phys. Rev. B **95**, 045117 (2017).
[39] Y.-J. Kao, Y.-D. Hsieh, and P. Chen, Journal of Physics: Conference Series **640**, 012040 (2015).
[40] N. J. Higham, Numerical Algorithms **15**, 227 (1997).
[41] P. Corboz, J. Jordan, and G. Vidal, Phys. Rev. B **82**, 245119 (2010).
[42] P. Corboz, R. Orús, B. Bauer, and G. Vidal, Phys. Rev. B **81**, 165104 (2010).
[43] I. Pižorn, L. Wang, and F. Verstraete, Phys. Rev. A **83**, 052321 (2011).
[44] Z. Y. Xie, H. J. Liao, R. Z. Huang, H. D. Xie, J. Chen, Z. Y. Liu, and T. Xiang, Phys. Rev. B **96**, 045128 (2017).
[45] J. Jordan, R. Orús, G. Vidal, F. Verstraete, and J. I. Cirac, Phys. Rev. Lett. **101**, 250602 (2008).
[46] M. Lubasch, J. I. Cirac, and M.-C. Banuls, New Journal of Physics **16**, 033014 (2014).
[47] M. P. Zaletel and F. Pollmann, arXiv preprint arXiv:1902.05100 (2019).

I. SUPPLEMENTARY MATERIAL

A. Schultz algorithm

Here, we provide further information regarding the accuracy of the Schulz iteration. We show this by evaluating the distance $F_{SC} = \| M^\dagger M - R^2 \|$ as a function of the Schulz iteration. The MPO compression (see Fig. 1(j)) is controlled by a bond dimension χ (in the final iteration in the canonicalization algorithm, this is always set to D). In Fig. 5(a), we show how the accuracy of the Schulz iteration depends on χ for different initial bond dimensions D for the ITF model at magnetic field $\lambda = 2.0$. The regularization parameter is always set to $\delta \sim 10^{-6}$.

B. Results for 2D Heisenberg model

The 2D Heisenberg model is defined by

$$H_{\text{Heisenberg}} = \sum_{\langle i,j \rangle} \mathbf{S}_i \cdot \mathbf{S}_j,$$

where $\mathbf{S}_i \equiv (\sigma_x, \sigma_y, \sigma_z)$ and σ_α are the Pauli matrices. Here we give additional results for the QR optimization. We have plotted the relative distance F versus iteration number for a single bulk column with $l_y = 10$ in Fig. 5(b). Note we have set the block size $l = 2$. The relative error of the norm contraction Δ is similar to that of the ITF model at the critical point ($\sim 10^{-2}$) for a lattice of size 10×10.

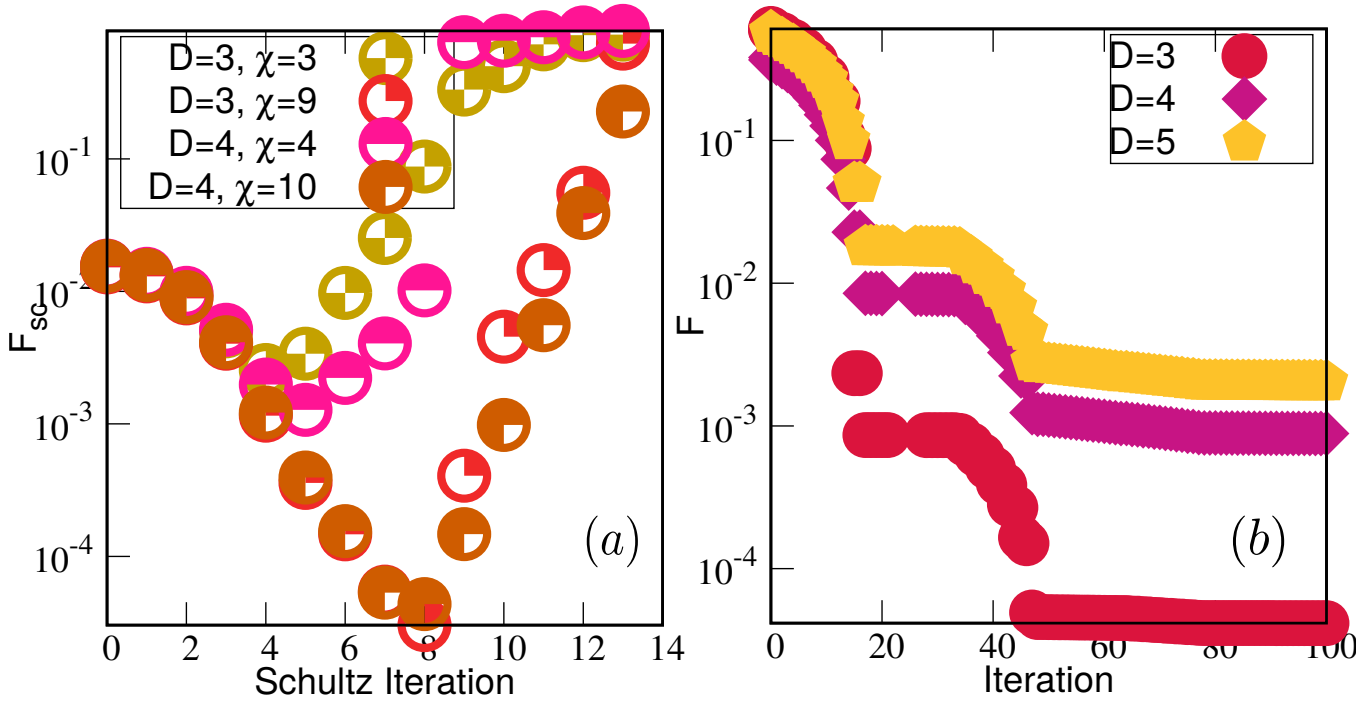

FIG. 5. (Color online) (a) The distance F_{SC} as a function of Schulz iteration for a single bulk column with $l_y = 16$ at magnetic field $\lambda = 2.0$. (b) The relative distance F of Heisenberg model versus iteration number of the QR optimization for a single bulk column with $l_y = 10$ and with different bond dimensions D.